A Pseudolite-Aided Navigation and Positioning Method for Complex Terrain Environments

Gang Zhao[1], Liwen Chen[2] Liangpeng Gao[1] and Xiaochun Cheng [3*]

[1]School of Transportation, Fujian University of Technology, Fuzhou, 350118, Fujian, China.
[2]School of Computer Science and Mathematics, Fujian University of Technology, Fuzhou, 350118, Fujian, China.
[3]Computer Science Department, Bay Campus，Fabian Way,Swansea University,Swansea, SA1 8EN Wales, UK.

Abstract—To address the challenges of degraded positioning accuracy, drift, or complete failure in environments where satellite signals are obstructed (e.g., basements, tunnels, canyons, forests, mountainous regions, and urban high-rise buildings), this paper proposes a navigation and positioning algorithm for complex terrains by integrating pseudolites with Time Difference of Arrival (TDOA) and trilateration techniques. First, to enhance the anti-interference capability and positioning accuracy of low-cost satellite receivers in conventional integrated navigation systems, we improve robustness and precision through the fusion of Global Navigation Satellite System (GNSS) and Inertial Measurement Unit (IMU) data. At the front-end processing stage, the algorithm calculates the relative positions and time differences between multiple pseudolites and receivers while integrating absolute position data derived from trilateration for state estimation, thereby providing accurate initial pose initialization for the back-end module. Subsequently, the back-end employs an Extended Kalman Filter (EKF) to fuse data from wheel odometry, GNSS, and IMU, optimizing the algorithm's accuracy and global consistency. Finally, the proposed algorithm is validated in high-dynamic motion scenarios and a comprehensive campus environment. Experimental results demonstrate that, compared to mainstream GNSS/IMU fusion methods and LiDAR-based Simultaneous Localization and Mapping (SLAM) algorithms, the proposed algorithm achieves superior positioning accuracy (with a root mean square error reduction of 58–72% in occluded scenarios) and exhibits enhanced robustness in aggressive motion conditions.

Index Terms—Pseudolite; Global Navigation Satellite System (GNSS); Extended Kalman Filter (EKF); Integrated Navigation; Multi-Sensor Fusion.

I. INTRODUCTION

The Global Navigation Satellite System (GNSS) is a space-based system that utilizes satellites orbiting the Earth combined with ground-based control infrastructure to deliver global Positioning, Navigation, and Timing (PNT) services [1], [2].It provides global coverage and high accuracy for outdoor positioning. However, GNSS signals are weak when reaching receivers due to their high orbital altitude and are susceptible to propagation-related interference [3].

In obstructed environments such as tunnels, urban areas, and mountainous regions, positioning accuracy degrades significantly because of signal blockage and multipath effects, sometimes leading to complete service denial [4], [5].Intentional interference further reduces GNSS reliability in civilian applications. To address these challenges, many nations have developed GNSS augmentation and backup systems for signal-degraded environments [6], [7].Ground-based pseudolite positioning systems, which apply similar principles to satellite navigation, provide an effective alternative in constrained environments. However, such systems still face challenges in algorithm design due to the limited number of available signals and complex error characteristics under occlusion conditions..

II. RELATED WORK

To address the challenges of precise navigation and localization in complex terrain environments, extensive research has been conducted on multi-sensor fusion methods. Cao et al. [8] proposed GVINS, a tightly coupled visual–inertial navigation system integrating raw GNSS measurements with VIO via nonlinear optimization. Forster et al. [9] improved VIO consistency using manifold-based preintegration and factor graph optimization. Wen and Hsu [10] developed a GNSS-RTK positioning framework based on factor graph optimization, demonstrating robustness but still limited in obstructed environments. Tao et al. [11] introduced a global pose graph optimization strategy combining visual, IMU, and GNSS data to enhance accuracy. Park [12] applied an adaptive unscented Kalman filter (A-UKF) for dynamic sensor fusion, improving accuracy but sensitive to noise modeling. Vizzo et al. [13] proposed Kiss-ICP for robust large-scale point cloud registration, while Zhang et al. [14] presented the CID-SIMS dataset for indoor multimodal sensing.

This paper proposes a navigation and localization algorithm for complex terrains based on pseudolite-fused Time Difference of Arrival (TDOA) and trilateration. Experimental results demonstrate that the proposed algorithm significantly enhances positioning performance under constrained conditions, providing stable and reliable localization.

A pseudolite is a ground-based device designed to generate and transmit navigation signals analogous to GNSS waveforms [15]. Pseudolite systems enhance GNSS performance in complex environments and provide independent positioning services in GNSS-denied scenarios [16]. Compared with GNSS satellites, pseudolites are deployed much closer to receivers, typically from several to hundreds of meters. Fig. 1 illustrates the schematic of a pseudolite positioning system consisting of space-based MEO satellites (e.g., GPS, BeiDou) and terrestrial pseudolites.

This study uses HackRF One SDRs to emulate pseudolite transmissions within a predefined area. Base stations are strategically placed with known coordinates to ensure positioning

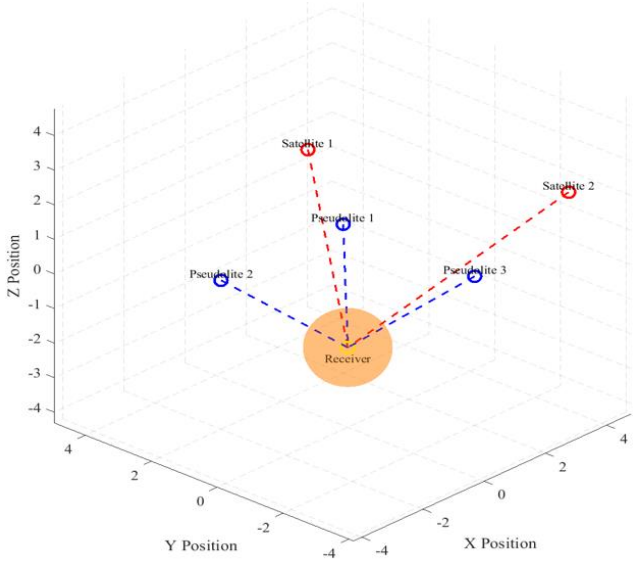

Fig 1. The Pseudolite System.

accuracy.

These systems can operate independently in GNSS-denied environments, such as underground or extraterrestrial scenarios, to provide Positioning, Navigation, and Timing (PNT) services. A key challenge is determining base station positions. To address this, Stanford proposed a Self-Calibrating Pseudolite Array (SCPA), where each node transmits and receives signals to achieve clock bias cancellation without external references [17].

III. SYSTEM ARCHITECTURE AND ALGORITHM DESIGN

The block diagram of the proposed pseudolite-fused Time Difference of Arrival (TDOA) and trilateration-based navigation and localization algorithm is illustrated in Fig. 2. The system architecture comprises multiple functional modules, including pseudolite ranging, inertial measurement, pseudolite base station data management, clock synchronization, measurement fusion, and navigation filtering.

A. System Description

In the pseudolite ranging module, the relative coordinates of the target are computed using the TDOA algorithm and cross-referenced with positional data from the pseudolite base station database to provide additional localization constraints.

The system integrates target motion predictions and performs clock synchronization via software-defined radio (SDR) devices (e.g., HackRF One) to resolve the receiver's absolute position. The trilateration algorithm further refines ranging accuracy by leveraging geometric relationships among multiple pseudolites.

The inertial measurement module employs an inertial measurement unit (IMU) with gyroscopes and accelerometers to acquire real-time kinematic states of the carrier. A sensor error compensation submodule corrects biases and drifts in raw IMU data, which are then fed into a navigation filter to iteratively update position and state estimates, mitigating cumulative errors and enhancing precision.

The pseudolite base station database stores pre-surveyed coordinates of pseudolites and ensures temporal consistency through clock synchronization protocols. The measurement fusion module.

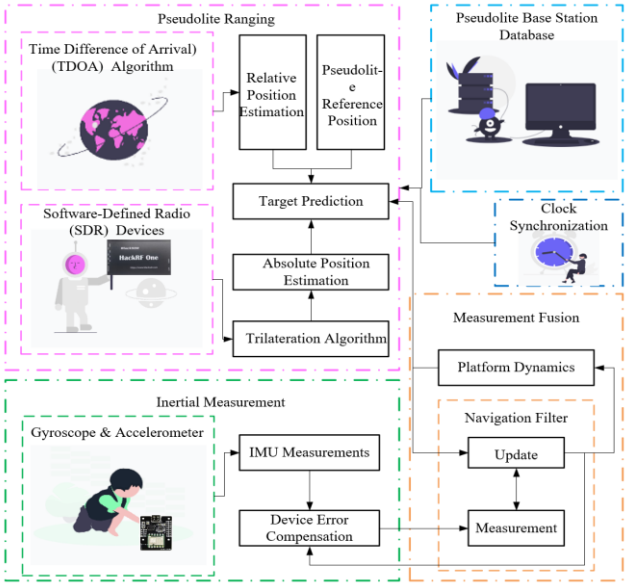

Fig 2. System Block Diagram of Pseudolite-Aided TDOA and Trilateration-Based Navigation and Positioning Algorithm.

combines pseudolite ranging data with IMU observations using weighted optimization to reconstruct the carrier's motion trajectory.

Within the navigation filtering module, an extended Kalman filter (EKF) updates the system state by incorporating discrepancies between pseudolite range measurements and IMU-predicted positions or velocities as innovations. The EKF estimates error parameters, compensates IMU biases, and optimizes localization outputs through recursive feedback.

This multi-sensor fusion framework improves the stability and accuracy of pseudolite-based navigation, enabling reliable positioning in indoor or GNSS-deprived environments.

B. Mathematical Model

In the pseudolite-based ranging module, the TDOA measurement observed by the user receiver is given by:

$$y_{i,k}^{TDOA} = (t_k^u - t_{i\,k}^s)c + \varepsilon_{i,k}^{TDOA} \quad (1)$$

Where t_k^u and $t_{i\,k}^s$ represent the reception timestamps at the user receiver and the i-th pseudolite transmitter, respectively; c denotes the speed of light; and $\varepsilon_{i,k}^{TDOA}$ denotes the TDOA measurement error.

The pseudorange observation from the i-th pseudolite transmitter at epoch k can ideally be represented as the dynamic geometric distance between the user receiver and the transmitter:

$$y_{i,k}^p = \left| r_{i,k}^s - r_k^u \right| + b_k^p + \varepsilon_{i,k}^p, i = 1,2,\ldots,N \quad (2)$$

Where b_k^p denotes the clock bias of the receiver at epoch k, $\varepsilon_{i,k}^p$ is the observation noise of the i-th pseudolite at epoch k, and N is the total number of pseudolite transmitters.

The IMU measurement model is given by:

$$y_k^{IMU} = g(X_k) + \varepsilon_k^{IMU} \quad (3)$$

Where $g(X_k)$ represents the state estimate obtained from the IMU, ε_k^{IMU} denotes the IMU measurement error.

In the navigation and positioning process, the unknown state vector X_k, including the position, velocity, clock bias, and frequency bias of

the receiver, needs to be estimated. This nonlinear filtering problem is addressed using an Extended Kalman Filter (EKF), which effectively handles nonlinear integration and provides better convergence and performance than traditional filters [18], [19].

The navigation and positioning system is modeled using an EKF, the observation equation is given by:

$$Z_k = h(X_k) + V_k \tag{4}$$

The state prediction is performed by: $X_{k|k-1}$,Which indicates the propagation of the previous state X_{k-1} to predict the current state X_k. The predicted covariance is calculated as:

$$P_{k|k-1} = F_k P_{k-1|k-1} F_k^T + Q_k \tag{5}$$

Where $P_{k|k-1}$ represents the state covariance matrix (indicating the uncertainty in the state estimate), The Kalman gain K_k is:

$$K_k = P_{k-1|k-1} H_k^T \left(H_k P_{k|k-1} H_k^T + R_k\right)^{-1} \tag{6}$$

Where H_k is the Jacobian matrix of the measurement function with respect to the state vector.The state update is performed via:

$$X_{k|k} = X_{k|k-1} + K_k\left(Z_k - h(X_{k|k-1})\right) \tag{7}$$

Where the term $Z_k - h(X_{k|k-1})$ is the innovation representing the difference between the actual measurement and its predicted value.

To further improve observation accuracy, outlier mitigation and adaptive modeling of the observation noise covariance are implemented as key innovations of the proposed approach.[20], [21].

IV. EXPERIMENTAL SETUP AND SCENARIOS

This chapter systematically elaborates the critical components of experimental design and implementation, establishing technical foundations for subsequent data acquisition and analysis.

A. Experimental Platform

All experiments were conducted using a custom four-wheeled robotic platform (Fig. 3), which integrates a Raspberry Pi 5 as the central processing unit, a WitMotion JY901B nine-axis IMU for inertial sensing, and a WTRTK-980 RTK module for positioning. A HackRF One software-defined radio (SDR) was employed as the pseudolite transmitter. The software framework was implemented in Linux using ROS for sensor integration and algorithm execution.

Fig 3. Experimental Platform.

B. Experimental Site And Pseudolite Deployment

Two representative test sites were selected: Site A, the underground parking lot of the library at Fujian University of Technology, and Site B, the corridor on the 5th floor of the College of Computer Science.

Fig 4. Site Layouts with Google Maps, On-Site Views, and Pseudolite Transmitter Positions (Sites A & B).

These locations represent environments with obstructed satellite signals, as shown in Fig. 4. Site A path: 26° 02′ 18″N, 119° 11′ 38″E to 26° 02′ 16″N, 119° 11′ 39″E, 100.26 meters. Site B path: 26° 02′ 21″N, 119° 11′ 31″E to 26° 02′ 20″N, 119° 11′ 29″E, 84.34 meters.

Three pseudolite transmitters were deployed at each site (A1, A2, A3 for Site A; B1, B2, B3 for Site B), as shown in Fig. 4, to optimize signal coverage and geometric dilution of precision (GDOP) under constrained base station quantities, ensuring robust positioning accuracy across diverse scenarios.

V. RESULTS AND DISCUSSION

To validate the proposed pseudolite-based navigation algorithm that fuses TDOA and trilateration, we conducted experiments under identical conditions as the GNSS/IMU and LiDAR/SLAM algorithms at Sites A and B. All experimental data were collected using the same platform, over the same time period, and along the same test trajectory. The resulting trajectories were then compared with the reference ground truth (Fig. 5). Therefore, all comparison results are based on fully consistent environmental and trajectory conditions, ensuring fairness and reproducibility of the evaluation.

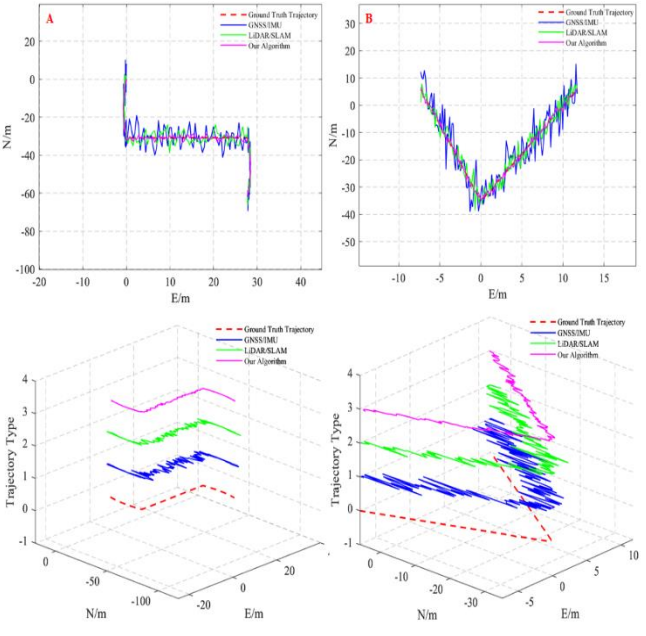

Fig 5. 2D and 3D Trajectory Comparison at Sites A and B

The GNSS/IMU solution suffers from multipath effects and IMU error accumulation in complex terrain (max deviation: 8 m), while LiDAR/SLAM achieves sub-meter accuracy in feature-rich areas but incurs cumulative errors (max offset: 5 m) in feature-sparse environments. The superior north-south error performance at Site A is likely attributed to the near-linear deployment of the four pseudolites along the tunnel's orientation (approximately north-south). This configuration leads to significantly lower positioning accuracy in the east-west direction compared to the north-south direction, as small timing errors in the TDOA measurements are substantially amplified perpendicular to the deployment axis.

Table 1. Comparison of Positioning Errors Among Algorithms in Complex Terrain at Sites A and B

Algorithm	MEAN(m)		RMSE(m)		STD(m)	
	SiteA	SiteB	SiteA	SiteB	SiteA	SiteB
GNSS/IMU	3.51	3.93	4.83	5.16	3.31	3.34
LiDAR/SLAM	2.59	2.60	3.07	2.98	1.78	1.46
Our Algorithm	1.22	0.89	1.40	1.11	0.69	0.66

The proposed algorithm, combining frontend multi-source fusion with backend enhanced EKF, achieves optimal global trajectory adherence with a mean absolute error of 0.7 m and local maxima not exceeding 1.4 m in severe signal-occluded zones. Positioning performance is evaluated using MEAN, RMSE, and STD metrics (Eqs. 8-10), with results summarized in Table I.

$$MEAN = \frac{1}{N}\sum_{k=1}^{N}\left\|X_k - X_k^{True}\right\| \tag{8}$$

$$RMSE = \sqrt{\frac{1}{N}\sum_{k=1}^{N}\left\|X_k - X_k^{TRUE}\right\|^2} \tag{9}$$

$$STD = \sqrt{\frac{1}{N}\sum_{k=1}^{N}\left(\left\|X_k - X_k^{TRUE}\right\| - MEAN\right)^2} \tag{10}$$

The proposed algorithm achieves MEAN errors of 1.22 m and 0.89 m in Sites A and B, respectively, with RMSE reduced to 1.40 m and 1.11 m. Compared to GNSS/IMU, it delivers average improvements of 71.25%, 74.75%, and 79.70% in MEAN, RMSE, and STD, respectively. Versus LiDAR/SLAM, improvements reach 59.34%, 58.58%, and 58.02%. In Scenario B with severe signal occlusion, RMSE reduction reaches 78.5%, as shown in Fig. 6. These results confirm the TDOA-trilateration fusion's effectiveness in improving positioning accuracy in signal-challenged environments.

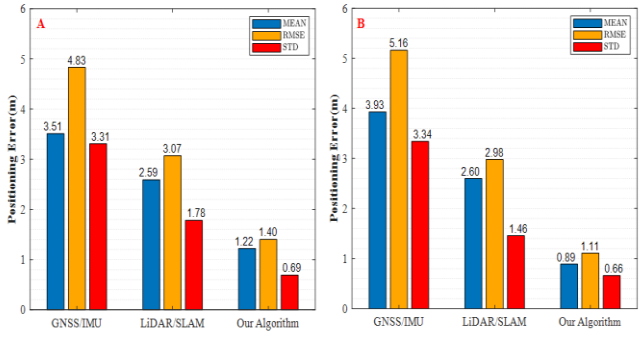

Fig 6. Positioning Performance Comparison of the Integrated Pseudolite-Based TDOA and Trilateration Algorithm in Complex Terrains.

REFERENCES

[1] T. H. Kindervatter and F. L. Teixeira, *Tropospheric and Ionospheric Effects on Global Navigation Satellite Systems*. Hoboken, NJ, USA: Wiley, 2022.

[2] P. D. Groves, "Principles of GNSS, inertial, and multisensor integrated navigation systems," *IEEE Aerosp. Electron. Syst. Mag.*, vol. 30, no. 2, pp. 26–27, Feb. 2015, doi: 10.1109/MAES.2014.14110.

[3] X. Chen, W. Gao, and J. Wang, "Robust all-source positioning of UAVs based on belief propagation," *EURASIP J. Adv. Signal Process.*, vol. 2013, no. 1, pp. 1–11, Dec. 2013.

[4] W. Tang, J. Chen, C. Yu, *et al*., "A new ground-based pseudolite system deployment algorithm based on MOPSO," *Sensors*, vol. 21, no. 16, pp. 5364–5377, Aug. 2021.

[5] X. Gan, C. Sheng, H. Zhang, *et al*., "Combination of asynchronous array pseudolites and GNSS for outdoor localization," *IEEE Access*, vol. 7, pp. 38550–38557, Mar. 2019.

[6] J. Chen, L. Zhao, C. Li, *et al*., "Design of clock synchronization based on wireless clock difference negative feedback for independent distributed pseudolite systems," in *Proc. IEEE 6th Adv. Inf. Technol., Electron. Autom. Control Conf. (IAEAC)*, Beijing, China, Oct. 2022.

[7] D. Yun and C. Kee, "Centimeter accuracy stand-alone indoor navigation system by synchronized pseudolite constellation," in *Proc. 16th Int. Tech. Meeting Satellite Division ION*, Portland, OR, USA, Sep. 2002, pp. 213–225.

[8] S. Cao, X. Lu, and S. Shen, "GVINS: Tightly coupled GNSS–visual–inertial fusion for smooth and consistent state estimation," *IEEE Trans. Robot.*, vol. 38, no. 4, pp. 2004–2021, Aug. 2022, doi: 10.1109/TRO.2022.3160014.

[9] C. Forster, L. Carlone, F. Dellaert, *et al*., "On-manifold preintegration for real-time visual-inertial odometry," *IEEE Trans. Robot.*, vol. 33, no. 1, pp. 1–21, Feb. 2017.

[10] W. Wen and L.-T. Hsu, "Towards robust GNSS positioning and real-time kinematic using factor graph optimization," in *Proc. IEEE Int. Conf. Robot. Autom. (ICRA)*, Xi'an, China, May 2021, pp. 5884–5890.

[11] X. Tao, B. Zhu, S. Xuan, *et al*., "A multi-sensor fusion positioning strategy for intelligent vehicles using global pose graph optimization," *IEEE Trans. Veh. Technol.*, vol. 71, no. 3, pp. 2614–2627, Mar. 2021.

[12] G. Park, "Optimal vehicle position estimation using adaptive unscented Kalman filter based on sensor fusion," *Mechatronics*, vol. 99, p. 103144, Mar. 2024.

[13] I. Vizzo, T. Guadagnino, B. Mersch, *et al*., "KISS-ICP: In defense of point-to-point ICP—Simple, accurate, and robust registration if done the right way," *IEEE Robot. Autom. Lett.*, vol. 8, no. 2, pp. 1029–1036, Feb. 2023, doi: 10.1109/LRA.2023.3236571.

[14] Y. Zhang, N. An, C. Shi, *et al*., "CID-SIMS: Complex indoor dataset with semantic information and multi-sensor data from a ground wheeled robot viewpoint," *Int. J. Robot. Res.*, vol. 43, no. 7, pp. 899–917, Jun. 2024, doi: 10.1177/02783649241234567.

[15] J. Wang, "Pseudolite applications in positioning and navigation: Progress and problems," *J. Glob. Positioning Syst.*, vol. 1, no. 1, pp. 48–56, 2002.

[16] B. Hofmann-Wellenhof, H. Lichtenegger, and J. Collins, *GPS Theory and Practice*, 5th ed. New York, NY, USA: Springer, 2000.

[17] E. A. Lemaster, *Self-Calibrating Pseudolite Arrays: Theory and Experiment*. Stanford, CA, USA: Stanford Univ., 2002.

[18] I. Arasaratnam and S. Haykin, "Cubature Kalman filters," *IEEE Trans. Autom. Control*, vol. 54, no. 6, pp. 1254–1269, Jun. 2009, doi: 10.1109/TAC.2009.2019800.

[19] B. Gao, G. Hu, Y. Zhong, *et al*., "Cubature Kalman filter with both adaptability and robustness for tightly-coupled GNSS/INS integration," *IEEE Sens. J.*, vol. 21, no. 13, pp. 14997–15011, Jul. 2021, doi: 10.1109/JSEN.2021.3072886.

[20] R. E. Kalman, "A new approach to linear filtering and prediction problems," *J. Basic Eng.*, vol. 82, no. 1, pp. 35–45, Mar. 1960.

[21] S. J. Julier and J. K. Uhlmann, "Unscented filtering and nonlinear estimation," *Proc. IEEE*, vol. 92, no. 3, pp. 401–422, Mar. 2004, doi: 10.1109/JPROC.2003.823141.